Magnetic structure and spin excitations in $BaMn_2Bi_2$

S. Calder,[1,*] B. Saparov,[2] H. B. Cao,[1] J. L. Niedziela,[3] M. D. Lumsden,[1] A. S. Sefat,[2] and A. D. Christianson[1]

[1]*Quantum Condensed Matter Division, Oak Ridge National Laboratory, Oak Ridge, Tennessee 37831, USA*

[2]*Materials Science and Technology Division, Oak Ridge National Laboratory, Oak Ridge, Tennessee 37831, USA*

[3]*Instrument and Source Division, Oak Ridge National Laboratory, Oak Ridge, Tennessee 37831, USA*

(Received 28 October 2013; published 19 February 2014)

We present a single-crystal neutron scattering study of $BaMn_2Bi_2$, a recently synthesized material with the same $ThCr_2Si_2$-type structure found in several Fe-based unconventional superconducting materials. We show long-range magnetic order, in the form of a G-type antiferromagnetic structure, exists up to 390 K with an indication of a structural transition at 100 K. Utilizing inelastic neutron scattering, we observe a spin gap of 16 meV, with spin waves extending up to 55 meV. We find these magnetic excitations are well fit to a J_1-J_2-J_c Heisenberg model and present values for the exchange interactions. The spin-wave spectrum appears to be unchanged by the 100 K structural phase transition.

DOI: 10.1103/PhysRevB.89.064417 PACS number(s): 78.70.Nx, 74.25.Ha, 75.50.Ee

I. INTRODUCTION

The discovery of unconventional superconductivity in Fe-based materials has stimulated intense interest in the condensed-matter-physics community and offers a new system, with the same square planar crystal motif as the cuprates, in which to investigate the underlying mechanism of unconventional superconductivity [1–3]. Driven by the initial discovery of superconductivity, several new Fe-based materials have been uncovered, for example, the 1111 phase (RFeAsO, with R = rare earth), 111 phase (AFeAs, with A = alkali metal), 11 phase (FeTe or FeSe), 122 phase (AFe_2As_2), and FeSe122 phase (AFe_2Se_2) [2,3]. The FeAs (or FeSe) layers are the common ingredient, and unlike the cuprates, it is possible to dope the Fe site and attain superconductivity. As a consequence, much work has been done on this, particularly in the 122 phase.

Recent interest has also focused on complete substitution of the Fe ion in the 122-type structure as an avenue both to search for new classes of superconducting materials and to probe why no superconductivity is attained despite often similar physics. One pertinent example, $SrCo_2As_2$, shows many similar features to the Fe-based 122 materials, but as yet no superconductivity has been uncovered upon doping from the cobalt parent side [4]. Additionally, the chromium-based material $BaCr_2As_2$ was shown to host itinerant antiferromagnetism that differs from the Fe-122 materials that remains upon doping and prohibits superconductivity [5,6].

Directly related to our investigation is the Mn-122 material $BaMn_2As_2$ that shows alternative behavior to both Co and Fe-122 materials as well as the cuprates. $BaMn_2As_2$ is a G-type antiferromagnet (AFM), $T_N = 625$ K, with no structural transition in the magnetic phase [7,8]. Investigations of $BaMn_2As_2$ have indicated properties in the intermediate regime between those of the itinerant AFe_2As_2 antiferromagnets and the local-moment antiferromagnetic insulator La_2CuO_4 parent superconductor. Indeed, doping $BaMn_2As_2$ in the form $Ba_{1-x}K_xMn_2As_2$ has been shown to result in an antiferromagnetic local-moment metal [9]. Therefore it has been suggested that Mn-122 compounds may be well placed to act as a bridge between Fe- and Cu-based unconventional superconductors [2].

Reference [10] reported the growth and characterization of single crystals of the new Mn-122 material, $BaMn_2Bi_2$, the first bismuthide with $ThCr_2Si_2$-type structure [space group $I4/mmm$, with $a = 4.4902(3)$ Å and $c = 14.687(1)$ Å]. $BaMn_2Bi_2$ is insulating with a small band gap of $E_g = 6$ meV, with metallic behavior achieved via hole doping with 10% K substitution on the Ba site [10]. Susceptibility measurements revealed an anomaly around 400 K consistent with magnetic ordering, with an additional apparent anomaly around 100 K that also corresponds to an upturn in the resistivity [10].

$BaMn_2Bi_2$ shows similar properties to $BaMn_2As_2$ and therefore may be similarly placed to act as a bridge between Fe- and Cu-based unconventional superconductors. Additionally, $BaMn_2Bi_2$ offers an alternative to arsenic-based materials and is amenable to the growth of suitably large single crystals for neutron scattering. Here we report the results of a single-crystal neutron diffraction investigation of $BaMn_2Bi_2$ through both the 400 and 100 K anomalies observed from bulk measurements. We then extend our exploration of the physical properties of $BaMn_2Bi_2$ to a study of the spin excitation spectrum by means of inelastic neutron scattering measurements. Our results support the postulate that the Mn-122 series hosts magnetic and insulating properties intermediate between Fe- and Cu-based materials, and we utilize our single-crystal inelastic neutron scattering results to provide detailed information on the magnetic exchange interactions and spin gap.

II. EXPERIMENTAL METHODS

A detailed description of the single-crystal growth and characterization of $BaMn_2Bi_2$ is presented in Ref. [10]. Single-crystal neutron scattering measurements were performed on the four-circle diffractometer (HB-3A) at the High Flux Isotope Reactor at Oak Ridge National Laboratory (ORNL). A single crystal of ~100 mg was measured in the temperature range 4 to 400 K, and the data were refined using FULLPROF to obtain crystal and magnetic structures. To attain a suitable

*caldersa@ornl.gov

mass (∼3 g) for inelastic neutron scattering measurements five single crystals were coaligned to within 1° in the (HHL) scattering plane. Utilizing the ARCS spectrometer at the Spallation Neutron Source (SNS), ORNL, inelastic neutron measurements were performed at 4 and 120 K with incident energies of 60, 100, 120, 250, and 500 meV. To examine the spin excitations in all reciprocal lattice directions the sample was rotated by 90° in 1° steps for measurements with an incident energy of 100 meV. The different angular data were combined, and subsequent cuts were performed with the HORACE software [11]. The instrument resolution varies with energy transfer, and this was accounted for in our fitting of the data through the use of an analytical function described in Ref. [12], taking into account our chosen setup and neglecting broadening effects from the sample. The inelastic energy resolution at an energy transfer of 50 meV is 1.56 meV for 100 meV incident energy.

III. RESULTS AND DISCUSSION

A. Magnetic and nuclear structure of $BaMn_2Bi_2$

We begin our investigation of $BaMn_2Bi_2$ with single-crystal four-circle neutron diffraction measurements. We performed measurements on several different nuclear reflections and found the refined structure to be consistent with the previously reported powder x-ray measurements [10]. From susceptibility measurements there is an anomaly around 400 K, attributed to magnetic ordering [10]. At low temperatures we observed scattered intensity at the (101) reflection, which is forbidden by the nuclear $I4/mmm$ space-group symmetry but is consistent with long-range AFM order. Therefore (101) defines the propagation vector for BaMnBi in $I4/mmm$ in the body-centered tetragonal notation, which transforms to $(\frac{1}{2},\frac{1}{2},\frac{1}{2})$ in primitive tetragonal notation. Following the temperature evolution of the intensity at the (101) reflection position from 4 to 400 K, we observe a magnetic transition at $T_N = 387.2(4)$ K, shown in Fig. 1. Considering the intensity of magnetic reflections in different Brillouin zones at 4 K within a model based on equal populations of domains for tetragonal symmetry and normalizing to the nuclear reflections, we were able to define the magnetic structure in $BaMn_2Bi_2$ as being G-type AFM, with the spins aligned along the c axis. The ordered moment at 4 K is $3.83(4)\mu_B$/Mn, reduced from the $5\mu_B$/Mn expected for the high-spin $S = 5/2$ of Mn^{2+}, nevertheless closer to a local-moment description relative to the itinerant Fe-based superconductors. The magnetic structure, and within error the ordered moment, is the same as for the related Mn-122 $BaMn_2As_2$ [7]. The observed magnetic structure in the Mn-122 compounds is distinct from the stripe order of the Fe-122 superconductors that is often associated with Fermi surface nesting. The alternative structures are likely a consequence of the anisotropy of the Mn ion controlling the spin direction, rather than an indication of a direct correlation between the suppression of superconductivity or the local vs itinerant nature of the magnetism. Nevertheless, it may be an indication of a more significant distinction, necessitating further investigation.

Both susceptibility and resistivity measurements on $BaMn_2Bi_2$ suggest a further transition around 100 K in Ref. [10]. The behavior of the (101) magnetic reflection in Fig. 1(a), however, shows no observable change in the magnetic structure near 100 K. Figure 1(b) shows the nuclear (008) reflection, with an anomaly at the same temperature as that observed in bulk measurements. Such a change is indicative of a subtle tetragonal to orthorhombic transition that is not observable as a peak splitting due to the instrument resolution but would be manifested in a change in the extinction and therefore the measured intensity of a nuclear reflection. A tetragonal to orthorhombic structural change is observed in several Fe-122 parent superconductors and is perhaps a prerequisite for attaining superconductivity. No structural change in the magnetic ordered phase has been observed in the related $BaMn_2As_2$.

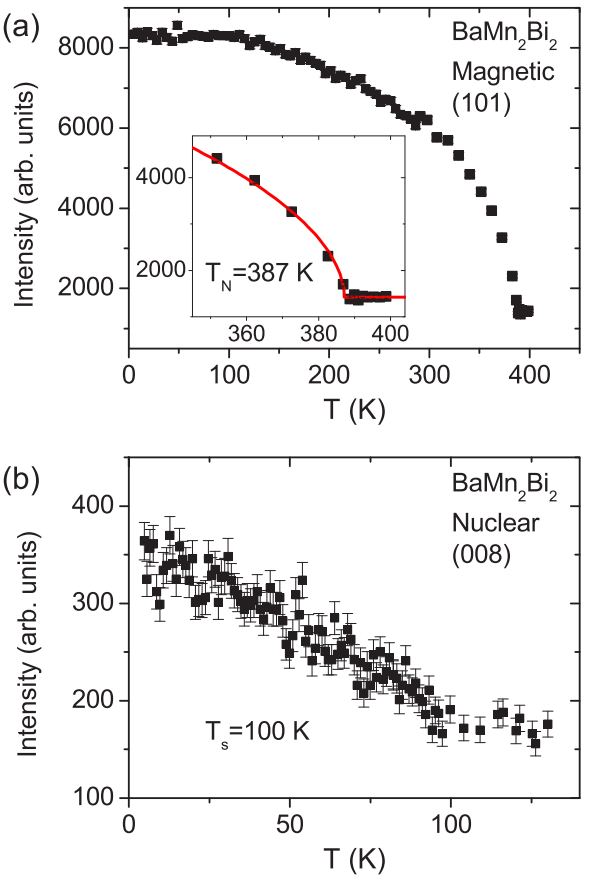

FIG. 1. (Color online) Single-crystal neutron scattering measurements on $BaMn_2Bi_2$. (a) Magnetic ordering occurs at (101) reflections, with the onset at 387.2(4) K. (b) A subtle structural transition is indicated by the change in the nuclear (008) reflection below 100 K.

B. Spin excitations of $BaMn_2Bi_2$

We now consider the magnetic excitations through a single-crystal inelastic neutron scattering experiment on ARCS with the aim of finding the exchange interactions and observing any spin gap, in addition to comparing excitations through the apparent 100 K structural transition. We performed an

initial survey using incident energies of $E_i = 60, 120, 250$, and 500 meV with the incident beam along the c axis. This allowed us to find the top of the spin excitations at ~60 meV and rule out any higher-energy spin waves. With the spin excitations residing around 60 meV and below we chose $E_i = 100$ meV to map out the low-Q Brillouin zones and performed cuts along high-symmetry directions. Constant energy cuts are shown in Figs. 2(a)–2(h) that follow the evolution of the low-energy excitations.

Familiar spin-wave cones are seen to develop centered on the magnetic Bragg points [Figs. 2(a)–2(d)], with overlapping excitations near the maximum of the branches [Figs. 2(e) and 2(f)]. The lack of any Q-dependent scattering in Fig. 2(b) at 10 meV indicates the existence of a spin gap in $BaMn_2Bi_2$. This is confirmed by an energy cut from the elastic magnetic Bragg reflection position (103), as shown in Fig. 2(i), where a distinct energy gap is observed well within the instrumental energy resolution of 2.7 meV at 5 meV energy transfer. No change in the gap is apparent through 100 K, where we observed a subtle structural transition from our single-crystal neutron diffraction. In order to fit the data we exclude the region near the elastic line and fit the resulting profile to a Gaussian convoluted with the instrument resolution to give an energy gap of $E_g = 16.29(26)$ meV at 5 K. The existence of a spin gap between $E_g = 6$ to 9 meV is a general feature of the inelastic neutron spectrum of parent Fe-122 materials [13,14], with debate existing as to the importance and consequence on the emergence of superconductivity. No spin gap is reported from the inelastic neutron scattering results of $BaMn_2As_2$ [8]. This may be a consequence of only polycrystalline $BaMn_2As_2$ being synthesized or, conversely, could point to different physics between the Mn-122 materials.

Figure 3 shows the energy variation and width through the spin waves at the zone boundary. The zone boundary energy is determined to be 34.2(3) meV, with a FWHM of 2.42(8) meV. With an instrument resolution at 34 meV of 1.9 meV this indicates sharp excitations, in contrast to what is observed for the Fe-122 materials, such as $BaFe_2As_2$ [15], that show diffuse scattering at the zone boundary. This distinction is likely an indication of a local-moment picture being more instructive for $BaMn_2Bi_2$ compared to the itinerant Fe-122 parent superconductors.

Theoretically, the spin gap is accounted for as a breaking of the Heisenberg spin rotation symmetry due to single-ion anisotropy in the model Hamiltonian, and we use this in our fitting method. We start from the Heisenberg Hamiltonian, which has proven effective for the low-energy excitations in the Fe-122 parent superconducting materials such as $CaFe_2As_2$ and $BaFe_2As_2$ [16,17]:

$$H = \sum_{\langle ij \rangle} (J_{ij}) S_i . S_j + \sum_{\langle i \rangle} D\left(S_z^2\right)_i, \quad (1)$$

where J_{ij} are exchange constants. We consider the ab-plane nearest-neighbor (J_1) and next-nearest-neighbor (J_2) interactions as well as the interaction from the c axis nearest neighbor (J_C), shown schematically in Fig. 4, with the spin-wave dispersion given by

$$E(q) = \sqrt{A(q)^2 - B(q)^2}. \quad (2)$$

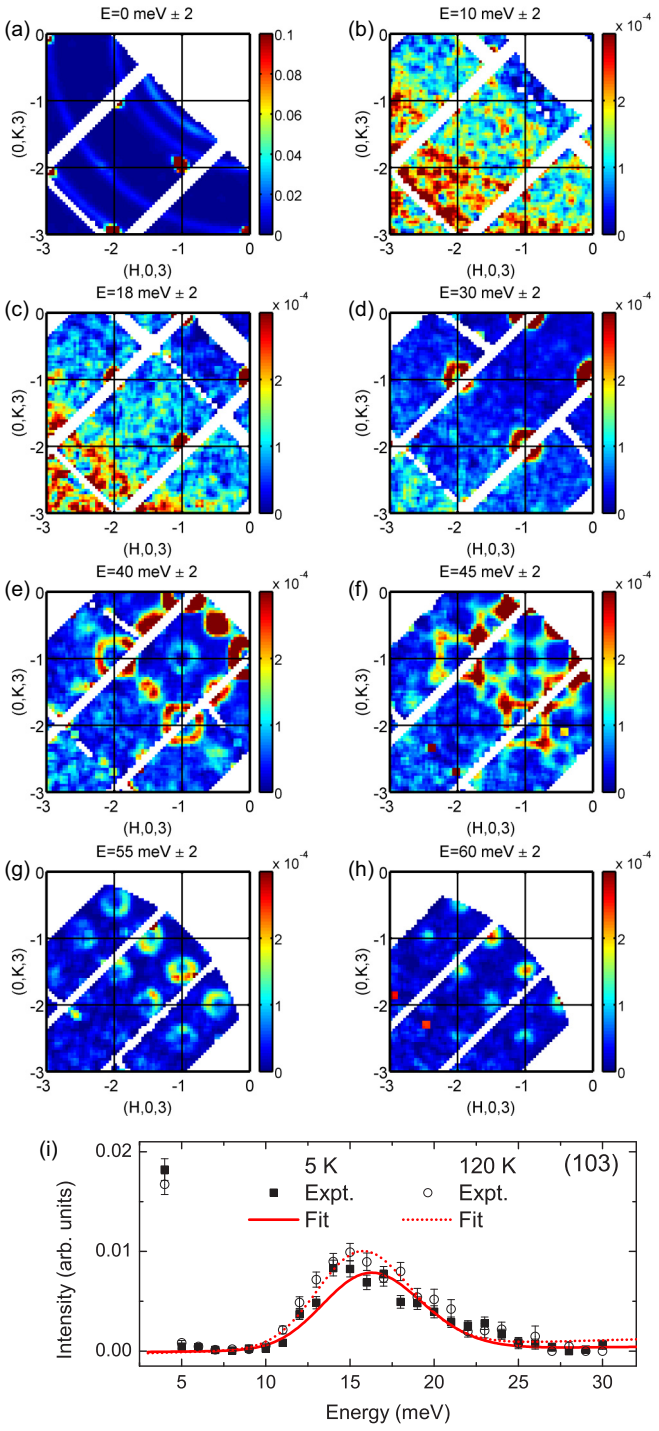

FIG. 2. (Color online) Inelastic neutron scattering measurements on single crystals of $BaMn_2Bi_2$ with an incident energy of 100 meV. (a)–(h) Constant energy cuts projected onto the (H,K) plane for fixed $L = 3$. The scale corresponds to intensity in arbitrary units. Excluding the $E = 0$ meV slice, the scale remains fixed for each plot. (i) Constant $q = (1,0,3)$ cut from the magnetic Bragg reflection in the range $(0.93 < H < 1.07, -0.07 < K < 0.07, 2.93 < L < 3.07)$ to reveal the spin gap.

In order to compare the exchange interactions with the related Mn-122 material $BaMn_2Bi_2$ and remain in tetragonal notation we use the form of dispersion presented by Johnston

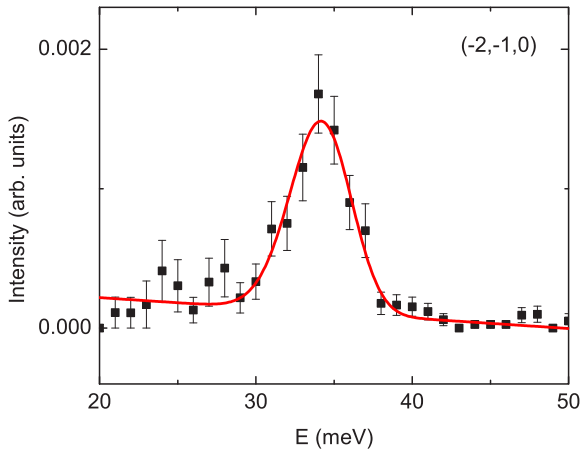

FIG. 3. (Color online) Energy variation showing the width of the excitation through the zone boundary at $(-2,-1,0)$ at 4 K. The fit is a Gaussian convolved with the instrument energy resolution.

et al. [8], with the addition of a single-ion-anisotropy term (D) due to the observed spin gap, with

$$A(q) = 2 + \frac{J_c}{J_1} - \frac{J_2}{J_1}[2 - \cos(2\pi H) - \cos(2\pi K)] + D, \tag{3}$$

$$B(q) = \cos[\pi(H+K)] + \cos[\pi(H-K)] + \frac{J_c}{J_1}\cos(\pi L), \tag{4}$$

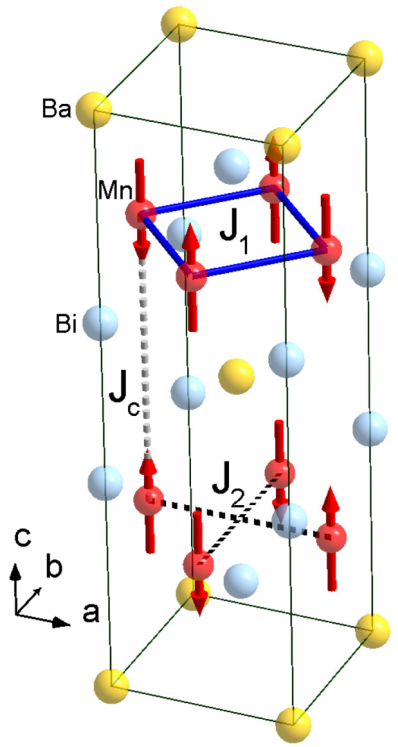

FIG. 4. (Color online) Crystal structure of $BaMn_2Bi_2$ with G-type AFM ordering of the Mn ions shown within the nuclear unit cell. The exchange interactions used in the model Hamiltonian correspond to J_1 (ab-plane nearest neighbor), J_2 (ab-plane next-nearest neighbor), and J_c (c-axis nearest neighbor).

where a and c are the tetragonal lattice constants of $BaMn_2Bi_2$ and the spin-wave energy is in units of SJ_1. This dispersion relationship is equivalent to those in Refs. [16,17]. For the case of G-type AFM with spins along the c axis the exchange interactions must satisfy the constraints that J_1 and J_C are positive and $J_1 > 2J_2$.

Figures 5(a) and 5(b) show the measured spin-wave dispersions projected onto high-symmetry directions in $BaMn_2Bi_2$. To obtain the exchange interaction values we took constant q cuts with varying energy transfer through the dispersions and fit the results with a Gaussian convolved with the instrument resolution to obtain the position of the dispersions. The results were then modeled with the dispersion relationship, Eq. (2), along both H and L directions to find the following unique set of exchange interactions that describe the magnetic spin excitations: $SJ_1 = 21.7(1.5)$, $SJ_2 = 7.85(1.4)$, $SJ_C = 1.26(0.02)$, $SD = 0.046(0.006)$. The exchange values are consistent with the constraints for G-type AFM ordering. Within the resolution of our measurements we do not find any change in exchange interactions between 4 and 120 K. Figures 5(c) and 5(d) show the calculated spin-wave dispersions and allow a comparison of both the position and intensity of the dispersions based on the model Heisenberg Hamiltonian. Starting with the standard expression for the neutron scattering cross section $S(\mathbf{Q},\omega)$ and following the treatment of parent superconducting compounds in Refs. [2,15,17,19] give the following expression for the intensity and position of the spin waves based on our model Hamiltonian:

$$S(\mathbf{Q},\omega) = S_{\text{eff}}\frac{4}{\pi}\frac{(A_q - B_q)}{E_0(1 - e^{-E/k_BT})}\frac{\Gamma E E_0}{\left(E^2 - E_0^2\right) + 4(\Gamma E)^2}, \tag{5}$$

where S_{eff} is the effective spin, E_0 is the dispersion energy, k_B is the Boltzmann constant, and Γ is the energy linewidth. In our calculations we additionally include the Mn^{2+} form factor and convolute the energy with the instrument resolution. Comparing the experimental and calculated intensities in Fig. 5 shows good qualitative agreement. Deviations, however, appear at the zone boundary for the intensity of the dispersions along L. This may be an indication of a departure from the Hamiltonian employed. Alternatively, given the good agreement for the H dispersion, the difference may instead be due to the calculation not taking into account the Q resolution of the measurement and, in particular, focusing effects that appear to be evident in the experimental results in Fig. 5(b). By considering the integrated intensities of the dispersions in Figs. 5(e) and 5(f) we find close agreement between experimental data and the calculation. This indicates that the Hamiltonian is a reliable model for the data and the apparent deviations between measured and calculated intensities between Figs. 5(b) and 5(d) are an artifact of the measurement.

Comparing the exchange interactions with those of $BaMn_2As_2$ reported in Ref. [8] shows a reduction in all values in $BaMn_2Bi_2$ and a lowering of the top of the observed excitations from 70 to 55 meV. The lowering of the excitations may be anticipated from the overall reduction in magnetic ordering temperature of $\sim$200 K from $BaMn_2As_2$ to $BaMn_2Bi_2$. The largest relative difference between the

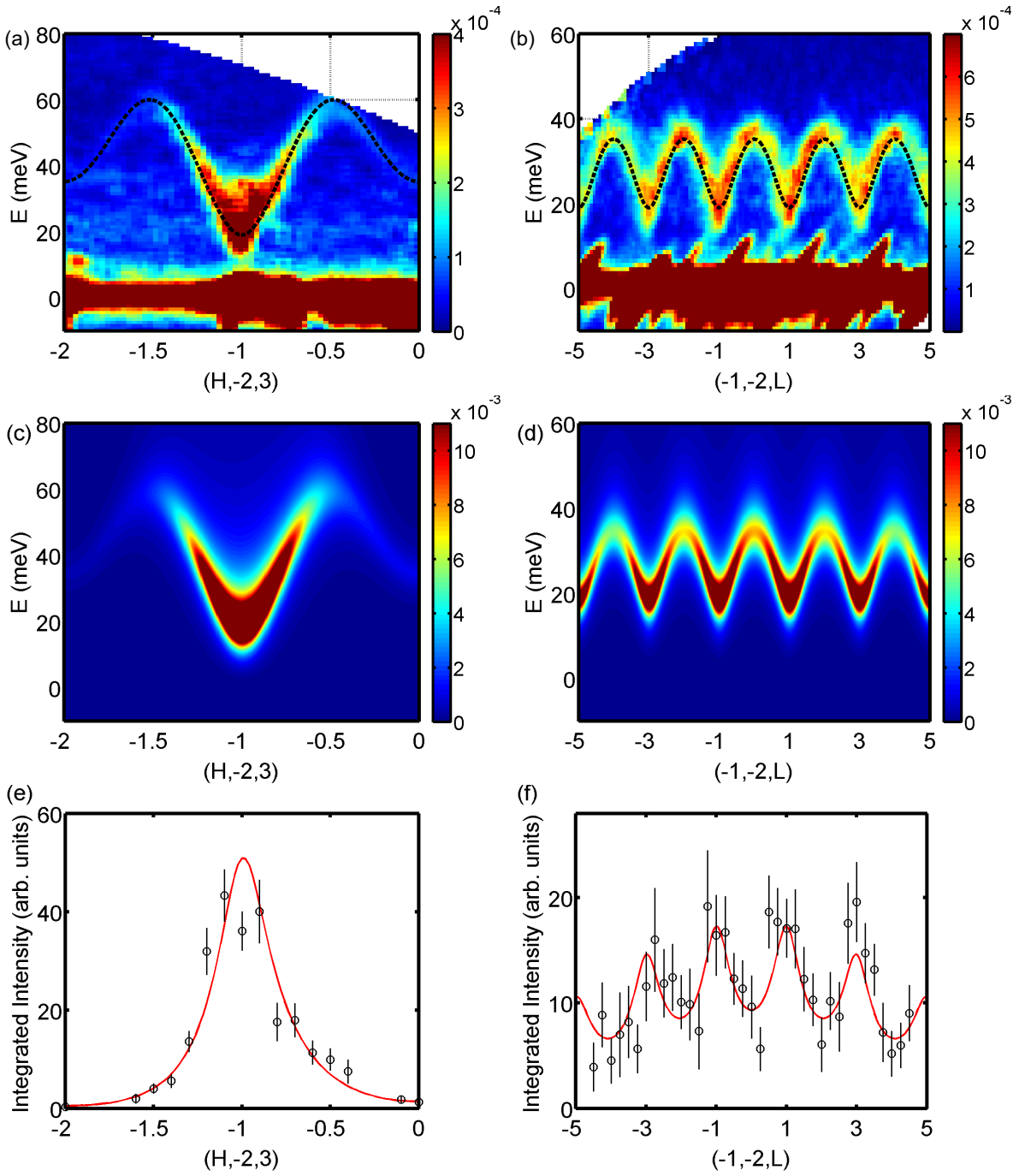

FIG. 5. (Color online) (a) and (b) Inelastic neutron scattering measurements on single crystals of $BaMn_2Bi_2$ show well-defined dispersions along high-symmetry directions. The intensity scale is in arbitrary units. The black dashed lines corresponds to the calculated dispersion relation using exchange interactions as described in the text. (c) and (d) The calculated dispersion position and intensity using the method described in the text. The intensity scale is mbr sr^{-1} meV^{-1} f.u. (e) and (f) Experimental (circles) and calculated (solid line) integrated intensity from constant **Q** scans through the dispersion curves.

exchange interactions is the reduction of the interaction along the c axis from 3 meV ($BaMn_2As_2$) to 1.26 meV ($BaMn_2Bi_2$). This may be explained in part as a consequence of the increase in the interplanar separation from 6.7 Å for the MnAs layers in $BaMn_2As_2$ to 7.3 Å for the MnBi layers in $BaMn_2Bi_2$ due to the c-lattice constant increase from 13.4149(8) Å ($BaMn_2As_2$) to 14.687(1) Å ($BaMn_2Bi_2$). However, the relative change of ∼8% is the same as the reduction in the Mn-Mn interplanar distance between $BaMn_2Bi_2$ and $BaMn_2As_2$, suggesting further mechanisms are important, such as the changes induced by the bismuth ion over the arsenic ion in the lattice.

Considering results for the exchange interactions in the J_1-J_2-J_c model for $CaFe_2As_2$ [13,18,19], $BaFe_2As_2$ [18,20], and $SrFe_2As_2$ [14,18], we find reduced values for all exchange interactions in the form SJ in $BaMn_2Bi_2$ apart from a lower

J_c value in $BaFe_2As_2$ but comparable single-ion anisotropy values. Therefore, in general, it appears the spin waves and exchange interactions in $BaMn_2Bi_2$ are lower in energy compared to 122 materials, even though the magnetic ordering temperature lies between $BaMn_2As_2$ and the Fe-122 materials. The overall divergence of the excitation energy and width, despite similarities such as the observed spin gap and structural transition in the magnetic phase, is a reflection of the differing underlying physical properties between $BaMn_2Bi_2$ and Fe-122 materials, and further investigations via doping would be of interest to follow the evolution of the excitations in this Mn-122 material.

IV. CONCLUSIONS

Neutron scattering measurements on single crystals have revealed $BaMn_2Bi_2$ forms a *G*-type AFM at 390 K with spins aligned along the *c* axis. We find an ordered moment of ∼75% compared to the expected spin-only value, indicating possible hybridization and divergence from pure local-moment behavior; however, $BaMn_2Bi_2$ appears to reside much closer to the local-moment limit than itinerant Fe-122 systems. Our single-crystal diffraction measurements suggest $BaMn_2Bi_2$ undergoes a subtle structural transition, similar to the Fe-122 materials but distinct from the related Mn-122 material $BaMn_2As_2$. A general feature of Fe-122 systems is the existence of a spin gap as observed in inelastic neutron measurements, while the underlying relationship, if any, to superconductivity remains an open question. Our measurements on gram-sized single crystals reveal well-defined spin waves and a gap of 16 meV in the low-energy excitations in $BaMn_2Bi_2$, not seen in $BaMn_2As_2$, which remains unchanged in the magnetic regime from 5 to 120 K. Indeed, the spin excitations show no apparent change through the structural transition. Applying a J_1-J_2-J_c Heisenberg model accounts well for the spin excitations and shows a lower energy scale compared to both $BaMn_2As_2$ and the Fe-122 materials. Overall, our results are consistent with the postulate that the Mn-122 materials host intermediate properties between the local-moment antiferromagnet insulating cuprate parent materials and itinerant antiferromagnetic Fe systems. Therefore in the context of investigating phenomena related to unconventional superconductivity $BaMn_2Bi_2$ appears to be well suited as a potential new bridging material.

ACKNOWLEDGMENTS

This research at ORNL's High Flux Isotope Reactor and Spallation Neutron Source was sponsored by the Scientific User Facilities Division, Office of Basic Energy Sciences, US Department of Energy. Research was supported by the US Department of Energy (DOE), Basic Energy Sciences (BES), Materials Sciences and Engineering Division (B.S., A.S.S.).

[1] Y. Kamihara, T. Watanabe, M. Hirano, and H. Hosono, J. Am. Chem. Soc. **130**, 3296 (2008).
[2] D. C. Johnston, Adv. Phys. **59**, 803 (2010).
[3] M. D. Lumsden and A. D. Christianson, J. Phys. Condens. Matter **22**, 203203 (2010).
[4] W. Jayasekara, Y. Lee, A. Pandey, G. S. Tucker, A. Sapkota, J. Lamsal, S. Calder, D. L. Abernathy, J. L. Niedziela, B. N. Harmon, A. Kreyssig, D. Vaknin, D. C. Johnston, A. I. Goldman, and R. J. McQueeney, Phys. Rev. Lett. **111**, 157001 (2013).
[5] D. J. Singh, A. S. Sefat, M. A. McGuire, B. C. Sales, D. Mandrus, L. H. VanBebber, and V. Keppens, Phys. Rev. B **79**, 094429 (2009).
[6] K. Marty, A. D. Christianson, C. H. Wang, M. Matsuda, H. Cao, L. H. VanBebber, J. L. Zarestky, D. J. Singh, A. S. Sefat, and M. D. Lumsden, Phys. Rev. B **83**, 060509 (2011).
[7] Y. Singh, M. A. Green, Q. Huang, A. Kreyssig, R. J. McQueeney, D. C. Johnston, and A. I. Goldman, Phys. Rev. B **80**, 100403 (2009).
[8] D. C. Johnston, R. J. McQueeney, B. Lake, A. Honecker, M. E. Zhitomirsky, R. Nath, Y. Furukawa, V. P. Antropov, and Y. Singh, Phys. Rev. B **84**, 094445 (2011).
[9] A. Pandey, R. S. Dhaka, J. Lamsal, Y. Lee, V. K. Anand, A. Kreyssig, T. W. Heitmann, R. J. McQueeney, A. I. Goldman, B. N. Harmon, A. Kaminski, and D. C. Johnston, Phys. Rev. Lett. **108**, 087005 (2012).
[10] B. Saparov and A. S. Sefat, J. Solid State Chem. **204**, 32 (2013).
[11] T. G. Perring, R. A. Ewings, and J. V. Duijn (unpublished), http://horace.isis.rl.ac.uk.
[12] D. L. Abernathy, M. B. Stone, M. J. Loguillo, M. S. Lucas, O. Delaire, X. Tang, J. Y. Y. Lin, and B. Fultz, Rev. Sci. Instrum. **83**, 015114 (2012).
[13] R. J. McQueeney, S. O. Diallo, V. P. Antropov, G. D. Samolyuk, C. Broholm, N. Ni, S. Nandi, M. Yethiraj, J. L. Zarestky, J. J. Pulikkotil, A. Kreyssig, M. D. Lumsden, B. N. Harmon, P. C. Canfield, and A. I. Goldman, Phys. Rev. Lett. **101**, 227205 (2008).
[14] J. Zhao, D.-X. Yao, S. Li, T. Hong, Y. Chen, S. Chang, W. Ratcliff, J. W. Lynn, H. A. Mook, G. F. Chen, J. L. Luo, N. L. Wang, E. W. Carlson, J. Hu, and P. Dai, Phys. Rev. Lett. **101**, 167203 (2008).
[15] L. W. Harriger, H. Q. Luo, M. S. Liu, C. Frost, J. P. Hu, M. R. Norman, and P. Dai, Phys. Rev. B **84**, 054544 (2011).
[16] S. O. Diallo, V. P. Antropov, T. G. Perring, C. Broholm, J. J. Pulikkotil, N. Ni, S. L. Bud'ko, P. C. Canfield, A. Kreyssig, A. I. Goldman, and R. J. McQueeney, Phys. Rev. Lett. **102**, 187206 (2009).
[17] R. A. Ewings, T. G. Perring, R. I. Bewley, T. Guidi, M. J. Pitcher, D. R. Parker, S. J. Clarke, and A. T. Boothroyd, Phys. Rev. B **78**, 220501 (2008).
[18] M. J. Han, Q. Yin, W. E. Pickett, and S. Y. Savrasov, Phys. Rev. Lett. **102**, 107003 (2009).
[19] J. Zhao, D. T. Adroja, D.-X. Yao, R. Bewley, S. Li, X. F. Wang, G. Wu, X. H. Chen, J. Hu, and P. Dai, Nat. Phys. **5**, 555 (2009).
[20] K. Matan, R. Morinaga, K. Iida, and T. J. Sato, Phys. Rev. B **79**, 054526 (2009).